Wave-Resistance Computation via CFD and IGA-BEM Solvers: A Comparative Study

Xinning Wang, Sotirios P. Chouliaras, Panagiotis D. Kaklis
Dept. Naval Architecture, Ocean and Marine Engineering (NAOME), University of Strathclyde
Glasgow, UK
Alexandros A.-I. Ginnis
Dept. Naval Architecture and Marine Engineering, National Technical University of Athens (NTUA)
Athens, Greece (GR)
Constantinos G. Politis
Dept. Naval Architecture, Technological Educational Institute of Athens (TEI-Athens)
Athens, GR
Konstantinos V. Kostas
Dept. Department of Mechanical Engineering, Nazarbayev University
Astana, Kazakhstan

ABSTRACT

This paper delivers a preliminary comparative study on the computation of wave resistance via a commercial CFD solver (STAR-CCM+®) versus an in-house developed IGA-BEM solver for a pair of hulls, namely the parabolic Wigley hull and the KRISO container ship (KCS). The CFD solver combines a VOF (Volume Of Fluid) free-surface modelling technique with alternative turbulence models, while the IGA-BEM solver adopts an inviscid flow model that combines the Boundary Element approach (BEM) with Isogeometric Analysis (IGA) using T-splines or NURBS. IGA is a novel and expanding concept, introduced by Hughes and his collaborators (Hughes et al, 2005), aiming to intrinsically integrate CAD with Analysis by communicating the CAD model of the geometry (the wetted ship hull in our case) to the solver without any approximation.

KEY WORDS: Computational Fluid Dynamics (CFD); Reynolds Averaged Navier Stokes (RANS) equations; Boundary Element Method (BEM), Isogeometric Analysis (IGA); wave resistance; Wigley ship; KRISO Container Ship (KCS).

INTRODUCTION

The prediction of wave resistance in naval architecture plays an important role in hull optimisation, especially for higher Froude numbers when wave-resistance's share in total resistance becomes higher. It is well known that the total resistance of a ship can be roughly decomposed into the sum of frictional, viscous-pressure and wave resistance. Model testing is commonly used to predict the resistance components for new ships (ITTC, 1987). With the recent improvements in CFD (Computational Fluid Dynamics) tools, CFD is likely to provide a decent alternative for saving time and money for the prediction of resistance for modern ship hulls. This is not, however, the case for ship-hull optimisation when the geometry is unknown, which increases drastically the overall computational cost and the significance of deviation between the *accurate* CAD model of a ship hull and its *discrete* approximation usually adopted by the CFD solvers.

An alternative lower-cost path for the wave-resistance estimation can be employed by appealing to the Boundary Element Method (BEM) for solving the Boundary Integral Equation (BIE), which results from adopting the so-called Neumann-Kelvin model for the flow around an object moving on the otherwise undisturbed free-surface of an inviscid and irrotational liquid; see, e.g., (Brard, 1972) and (Baar and Price 1988). Our purpose is to initiate a systematic comparative study between a CFD solver (STAR-CCM+) and an in-house BEM solver enhanced with the IGA concept, which permits to tightly integrate the CAD model of a ship hull and its IGA-BEM solver; see, e.g. (Belibassakis et al 2013). Under the condition that this study will secure that the discrepancy between the results provided by the two solvers are acceptable within the operational range of Froude numbers, one can proceed to develop a hybrid mid-cost optimisation framework that combines appropriately the low-cost IGA-BEM solver (Kostas et al, 2015) with the high-cost CFD one. In the present paper our comparison will involve two hulls, namely the Wigley and the KCS hull, which have been extensively used in pertinent literature for experimental and computational purposes.

CFD SOLVER: METHODOLOGY AND SETUP

NAOME has provided (to the first three co-authors) access to the commercial CFD solver STAR-CCM+®, which uses a finite-volume method for capturing the free-surface elevation created by an object moving with constant velocity on the otherwise undisturbed free-surface of viscous incompressible fluid. This method uses a *Volume of Fluid (VOF)* approach based on integrating the incompressible *Reynolds time – averaged Navier-Stokes (RANS)* equations (Eq. 3, 4) over a control volume. Recall that the Navier-Stokes equations can be written as:

$$\rho\left(\frac{\vartheta V}{\vartheta t}+(V\cdot\nabla)V\right)=-\nabla P+\mu\nabla^2 V+f \quad (1)$$

$$\frac{\partial V_1}{\partial x}+\frac{\partial V_2}{\partial y}+\frac{\partial V_3}{\partial z}=0, \quad (2)$$

where $V=(V_1,V_2,V_3)$ is the fluid-velocity vector, ρ is the fluid density, μ is the dynamic viscosity and f represents the external forces acting on the fluid. The associated RANS equations can then be written in tensor form as:

$$\frac{\partial Ui}{\partial t}+\frac{\partial}{\partial x_j}(U_iU_j)=-\frac{1}{\rho}\frac{\partial p}{\partial x_i}+\frac{\partial}{\partial x_j}(2\nu S_{ij}-\overline{u_i'u_j'}), \quad (3)$$

$$\frac{\partial U_i}{\partial x_i}=0, \quad (4)$$

where U_i stands for the mean flow velocity component (i=1,2,3), ν is the kinematic viscosity, S_{ij} is the mean strain-rate tensor given by:

$$S_{ij}=\frac{1}{2}\left(\frac{\vartheta U_i}{\vartheta x_j}+\frac{\vartheta U_j}{\vartheta x_i}\right) \quad (5)$$

and, finally, $\overline{u_i'u_j'}$ is the Reynolds stress tensor R_{ij}. The well-known c*losure problem* of RANS equations consists in modelling the Reynolds stress tensor as a function of the mean velocity and pressure, in order to remove any reference to the fluctuating part of the velocity. In this work we employ two of the most common turbulence models used in CFD, namely the *k-epsilon (k-ε)* model and the *k–omega (k–ω)* model. The *k-epsilon* model is a two equation model which gives a general description of turbulence by means of two transport partial differential equations; see, e.g., (Launder and Spalding 1974). The *k–omega* model attempts to predict turbulence by two partial differential equations in terms of two variables, namely k and ω, with k being the turbulence kinetic energy while ω is the specific rate of dissipation of the turbulence kinetic energy k into internal thermal energy; see, e.g., (Wilcox 2008).

Locating the free surface in the two-phase (air, liquid) flow, created by the movement of a body on the free-surface of a fluid, can be materialised via the so-called *Volume Fraction Transport* equation (Peric & Ferziger, 2002) given below

$$\frac{\partial c}{\partial t}+\frac{\partial(cU_j)}{\partial x_j}=0, \quad (6)$$

where the volume fraction c is equal to V_{air}/V_{total} and the fluid density ρ is equal to

$$\rho=\rho_{air}c+\rho_{water}(1-c), \quad (7)$$

$$\mu=\mu_{air}c+\mu_{water}(1-c). \quad (8)$$

According to the standard practice, the total resistance of a ship is subdivided into two components, namely:

$$C_T=C_F+C_R, \quad (9)$$

where $C_T$is the total resistance coefficient, C_F is the friction resistance coefficient and C_R is the residual resistance coefficient. The friction resistance coefficient depends only on Reynolds number R_n and assumed to be independent from the residual resistance coefficient. Residual resistance (coefficient) can be further decomposed into wave resistance C_W and viscous pressure resistance C_{VP} coefficients, resulting in:

$$C_T=C_F+C_{VP}+C_W. \quad (10)$$

In the context of the the resistance test method adopted by the International Towing Tank Conference (ITTC) on 1978, the concept of *form-factor k* has been introduced, based on two assumptions, i.e., invariance between the model and the full-scale ship and invariance with respect to the Froude number *Fr*. Working in this context, we can write

$$C_{VP}=kC_F, \quad (11)$$

which results in:

$$C_T=(1+k)C_F+C_W. \quad (12)$$

For the two case studies undertaken in this paper, the form-factor for the Wigley hull will rely on experimental values from (Ju 1983) while the form-factor for the KCS hulls will be based on experimental results and CFD estimates.

Wigley hull is a biquadratic surface expressed analytically as:

$$y(x,z)=\frac{B}{2}\left\{1-\left(\frac{2x}{L}\right)^2\right\}\left\{1-\left(\frac{z}{T}\right)^2\right\}, \quad (13)$$

where L=4.0m (length between perpendiculars), B=0.4m (breadth), T=0.25m (draft), while x identifies the distance from mid-ship (positive towards bow), y denotes the distance from the symmetry plane and z denotes the distance measured from the undisturbed free-surface.

The second case study is a model of the so-called KCS (KRISO container ship) with main particulars given in Table 1. The CFD solver is using the NURBS-based CAD model (see Fig. 1) of the KCS ship which is available at the web-site of NMRI (National, Maritime Research Institute) of Japan[1]. For the needs of the IGA-BEM solver a new CAD model (see Fig. 2), as a multi patch NURBS model of the KCS model has been rebuilt for the hull below the waterline. This CAD model comprises bi-cubic patches and possesses first-order (G^1) geometric continuity globally, i.e., continuously varying unit normal. The surface is generated with a lofting (skinning) scheme on mid-body sections where the remaining stern/bow patches are the result of Gordon surface constructions on the corresponding sections, waterlines and/or stern/bow profile parts. The deviation between the two CAD models below the design waterline, measured in terms of integral geometric characteristics, is indeed very small, i.e., wetted-surface deviation: 0.076%, volume deviation: 0.055%, centroid deviation: (-0.010, 0.000, -0.037)%.

Table 1. Main particulars of the KCS ship

	scale ratio	Lpp (m)	Lwl (m)	Bw (m)	D (m)	T (m)
KCS ship	1/31.6	7.27	7.357	1.019	0.601	0.342

[1] https://www.nmri.go.jp/institutes/fluid_performance_evaluation/cfd_rd/

Fig. 1: Original CAD model of the KCS ship model

Fig. 2: Rebuilt CAD model of the KCS ship model

Meshing in the 2-phase flow region is undertaken by the adopted CFD solver enabling us to create trimmed hexahedral grids and prism layers along walls. Trimmed grids allow anisotropic local refinement around the hull and the free-surface. Representative 2D intersections of the developed meshes with appropriate planes are given in Figs. 3 to 6 while Tables 2 and 3 provide mesh-size information.

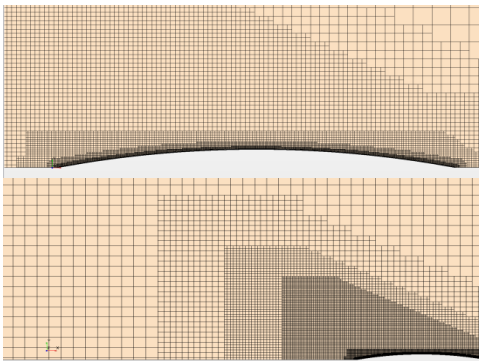

Fig. 3: Top-view of the mesh around the Wigley hull, showing different levels of refinement in the Kelvin-angle cone.

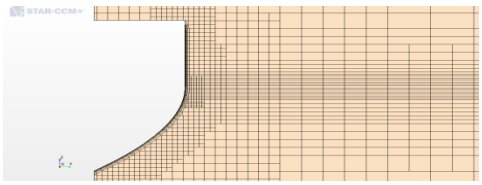

Fig. 4**:** Transverse intersection of the mesh around the midship section of the Wigley hull, showing local refinement near the free-surface.

Table 2. Fine-mesh information of the Wigley ship

min. element size	0.06 (m)
max element size	0.48 (m)
# elements	1,648,435

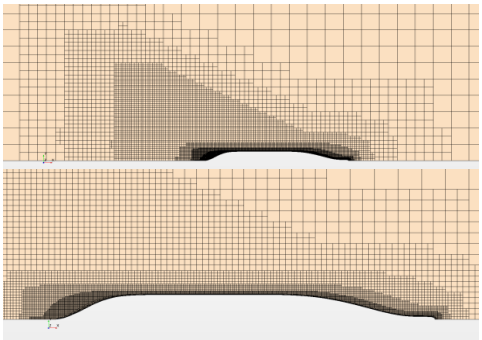

Fig. 5: Top-view of the mesh around the KCS hull, showing different levels of refinement in and around the Kelvin-angle cone.

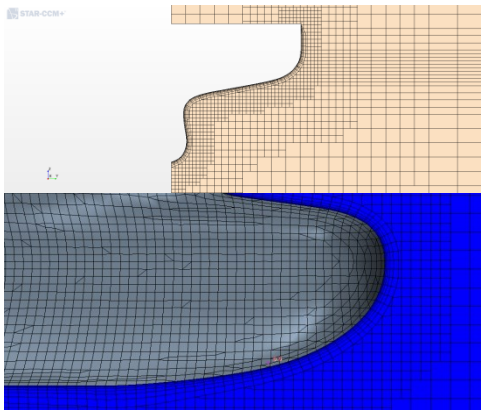

Fig. 6: Transverse intersection of the mesh around a stern section (upper) and a center-plane intersection of the mesh around the bulbous bow (lower) of the KCS hull.

Table 3. Fine-mesh information of the KCS ship

min.element size	0.056 (m)
max element size	0.896 (m)
# elements	2,115,022

Taking into account the symmetry of the flow with respect to the centre plane, the axes-aligned bounded boxes, used for by the CFD solver as computational domain, is the box [-5L,2.5L]x[0L,3.75L]x[-3.75L,2L] for the Wigley hull and the box [-2.47L,2.47L]x[0L,2.47L]x[-2.47L,1.24L] for the KCS ship hull, with L denoting the length of the corresponding hull. On the boundary of these computational boxes the typical boundary conditions in CFD problems are imposed, such as, inlet/outlet, wall, constant-pressure, symmetry boundary conditions, etc.

In order to choose the appropriate element base size and turbulence model, CFD results will be compared against available experimental results for Froude number Fr=0.267 for the Wigley hull and Fr=0.26 for both the original and the rebuilt KCS hulls. For this purpose, the CFD tool is used to compute the total force acting on the hull in the direction of its motion (x-direction) and then non-dimensionalised using the below formula, where Aw is the static wetted surface area of the hull and U_0 is the tow velocity.

$$C_T = \frac{R_T}{0.5\rho A_w U_0^2} \tag{14}$$

Experimental results for the Wigley hull are available in (Ju 1983), where U_0=1.67m/s, $Aw=Cs \bullet L(2D+B)$, Cs=0.661, and C_T=4.16x10^{-3} where C_T denotes the total-resistance coefficient. For the KCS hull: Aw= 9.4379 m^2 and U_0=2.196 m/s. Appealing to (Kim et al 2001), we have that C_T=3.557x10^{-3} while the frictional-resistance coefficient, C_F, is calculated using the ITTC correlation line (ITTC, 2008a) resulting in C_F =2.832x10^{-3}. The following three tables summarise a grid sensitivity analysis of the three test hulls with respect to the base size of the mesh adopted by the CFD tool and the employed turbulence models. Refinement is based on the pattern coarse_size=√2 medium_size=2 fine_size as recommended by ITTC (2008b). Tables 4 and 5 indicate that, for the k-e turbulence model, percentage error decreases as we move from coarse to fine mesh, which is however achieved via a dramatic increase in time cost. For the KCS test case the significant decrease of percentage error should be attributed to the "alignment" of fine mesh with the "needs" of the turbulence model. On the other hand, the error seems to be mesh-invariant for the turbulence model of Table 6.

Table 4. Grid sensitivity analysis for the Wigley hull (Fr=0.267, k-ε turbulence model)

grid	base size(m)	#cells (M)	$C_T \cdot 10^3$(error%)	time (h/m)
coarse	0.1200	0.48	3.83(-7.87%)	3/15
medium	0.0850	0.77	3.90(-6.25%)	6/12
Fine	0.0600	1.6	4.35(4.46%)	10
experimental value: C_T=4.16x10^{-3}, #cores=12				

Table 5. Grid sensitivity analysis for the KCS hull (Fr=0.26, k-ε turbulence model)

grid	base size (m)	# cells (M)	$C_T \cdot 10^3$(error%)	time (h/m)
coarse	0.1125	0.86	3.85(8.23%)	4/8
medium	0.0800	1.7	3.78 (6.15%)	10/11
fine	0.0560	2.1	3.54(-0.51%)	16/30
experimental value: C_T =3.557x10^{-3}, #cores=12				

Table 6. Grid sensitivity analysis for the KCS hull (Fr=0.26, Shear Stress Transport (SST) eddy viscosity model blending a variant of the k-ω model in the inner boundary layer and a transformed version of the k-ε model in the outer boundary layer and the free stream)

grid	base size (m)	# cells (M)	$C_T \cdot 10^3$(error%)	time (h/m)
coarse	0.1125	0.86	3.79 (6.68%)	5/10
medium	0.0800	1.7	3.74(5.03%)	8
fine	0.0560	2.1	3.80 (6.70%)	16
experimental value: C_T =3.557x10^{-3}, #cores=12				

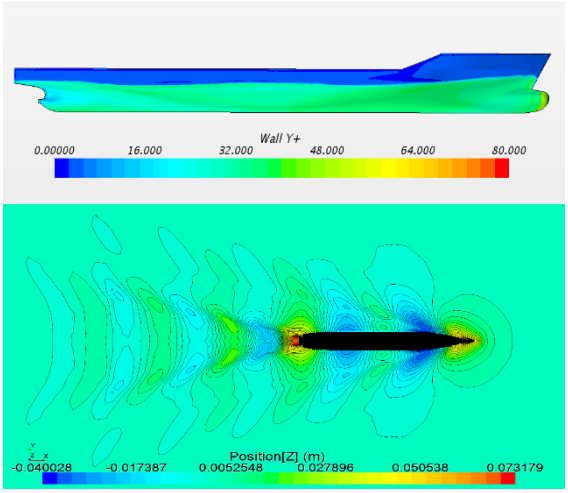

Fig. 7: Near-wall y+ values (expected to vary in the range 30-100) and the Kelvin wave-pattern distribution (fine base size, Fr=0.26 and k-ε turbulence model)

Finally, the ensuing three figures illustrate the performance of the CFD solver for estimating the wave/total and residual resistance of the Wigley and KCS hull against experimental results provided in (Ju 1983) and (Choi et al 2011), respectively. The wave resistance estimate in Fig. 8 is obtained by subtracting from the computed total-resistance coefficient the viscous resistance approximated by $(1+k)C_F$, where C_F is the well-known ITTC-57 friction-resistance estimate and k=0.08, which is obtained by applying Prohaska's method in conjunction with CFD total resistance estimates for small Froude numbers. Note that k=0.1 according to an experimental study available in (Ju 1983). As for Fig. 10, the CFD estimate of the residual resistance is obtained by subtracting from the total-resistance coefficient C_T the frictional-resistance coefficient C_F, evaluated again via the ITTC-57 formula.

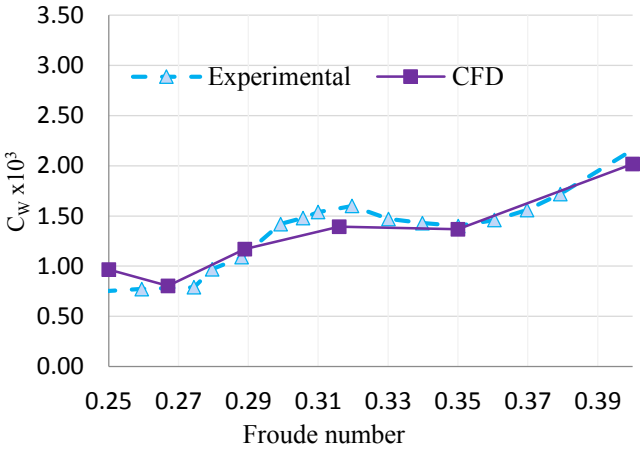

Fig. 8: Comparison of the wave-resistance CFD estimate against experimental results for the Wigley hull.

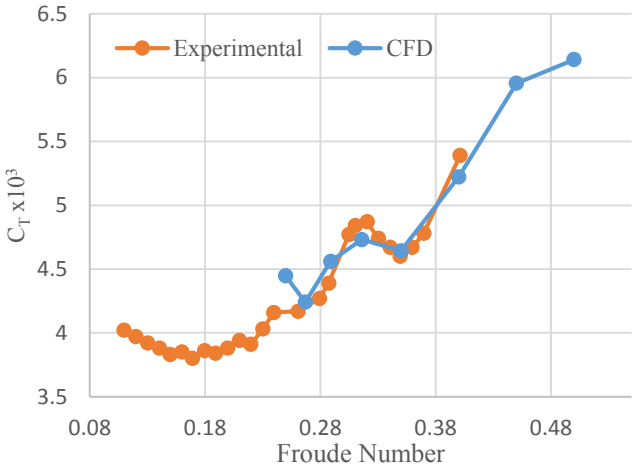

Fig. 9: Comparison of the total-resistance CFD estimate against experimental results for the Wigley hull.

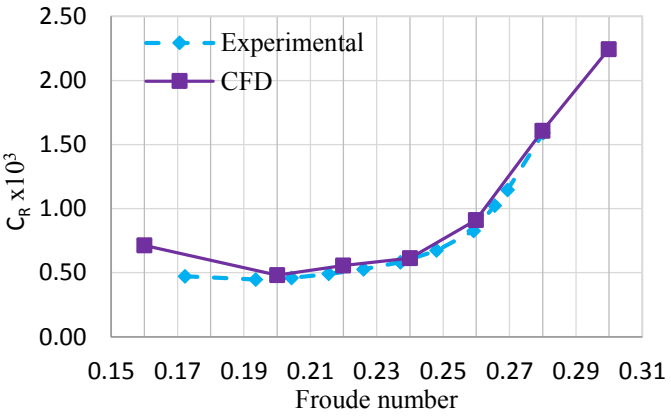

Fig. 10: Comparison of the residual-resistance CFD estimate against experimental results for the KCS hull.

IGA-BEM WAVE-RESISTANCE SOLVER

This paper follows the approach by Belibassakis et al (2013) based on the formulation by Brard (1972) and Baar and Price (1988). The ship-hull sails through an incompressible and inviscid fluid with a uniform velocity vector **U**=(-U,0,0). The flow is considered irrotational and a fixed-body coordinate system is used; see Fig. 11. The total velocity of the flow consists of the uniform velocity and the perturbation velocity due to the existence of the hull. The problem can be formulated by the weakly singular BIE,

$$\frac{\mu(P)}{2}-\int_S \mu(Q)\frac{\partial G(P,Q)}{\partial n(P)}dS(Q)-\frac{1}{k}\int_\ell \mu(Q)\frac{\partial G^*(P,Q)}{\partial n(P)}n_x(Q)\tau_y(Q)d\ell \qquad \mathrm{J}\cdot\mathbf{n}(P),$$

$$P,Q\in S \tag{15}$$

where μ is the density of the source distribution on the hull surface, G is the Neumann-Kelvin Green's function corresponding to a point source moving with velocity U on the undisturbed free surface. Furthermore, G^* is the regular part of Green's function, k is the characteristic wave number, n is a vector normal to the boundary surface S on point P, ℓ corresponds to the waterline and n_x and τ_y are the vectors normal and tangent to the waterline respectively on point Q.

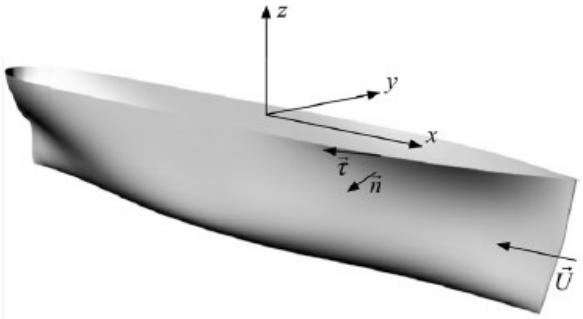

Fig. 11: Fixed-body coordinate system

The surface of the hull is represented as a tensor product multi-patch NURBs surface:

$$\mathbf{x}(t_1,t_2)=\sum_{i_1=0}^{n_1^p}\sum_{i_2=0}^{n_2^p}\mathbf{d}_{i_1i_2}^p R^p_{i_1i_2,k_1^pk_2^p}(t_1,t_2)\coloneqq\sum_{\mathbf{i}=0}^{\boldsymbol{n}^p}\mathbf{d}_{\mathbf{i}}^p R_{\mathbf{i}}^p(t_1,t_2), \tag{16}$$

where $\mathbf{d}_i^p$ are the control points of patch p, R_{i}^p are the standard rational B-spline basis functions, t_1, t_2 are the knot values for each parametric direction $\boldsymbol{n}^p=(n_1^p,n_2^p)$ where n_1^p, n_2^p are the number of bases functions for each parametric direction.

Following the concept of Isogeometric-Analysis (IGA) (Hughes 2005), the unknown source density distribution μ will be represented by using the same rational B-spline functions that were used for the ship hull surface:

$$\mu(t_1,t_2)=\sum_{\mathbf{i}=0}^{\mathbf{n}^p+\mathbf{l}^p}\mu_{\mathbf{i}}^p R^p_{\mathbf{i},\mathbf{l}^p}(t_1,t_2),\qquad (t_1,t_2)\in I_1^p\times I_2^p, \tag{17}$$

where $\mu_{\mathbf{i}}^p$ are the unknown source density coefficients and $\mathbf{l}^p=(\mathrm{l}_{\mathrm{i},1}^p,\mathrm{l}_{\mathrm{i},2}^p)$ where $\mathrm{l}_{\mathrm{i},1}^p,\mathrm{l}_{\mathrm{i},2}^p$ are the numbers of added knots for each parametric direction. The accuracy of this method depends on the number of the source density coefficients which are essentially the degrees of freedom (DoFs) of the numerical procedure. Consequently, a number of DoFs may be added by knot insertion given by $\mathbf{l}^p$ in order to get a more accurate approximation of the solution. The total number of DoFs is given by

$$M=\sum_p\left(n_1^p+l_1^p+1\right)\left(n_2^p+l_2^p+1\right) \tag{18}$$

Eq. 15 will be numerically solved by applying a collocation point scheme where each collocation point P_{j}^p on the physical space corresponds to the so-called Greville abscissae Farin (1999) of the associated knot vectors.

For each collocation point P_{j}^p, the induced velocity factor can be evaluated by

$$\mathbf{u}_{\mathrm{i}}^q\left(P_{\mathrm{j}}^p\right)=\int_{\Omega_{\mathrm{i}}^q}R^q_{\mathrm{i},\mathbf{l}^q}(t_1,t_2)\left[\nabla_p G\left(P_{\mathrm{j}}^p,\mathbf{x}(t_1,t_2)\right)\right]\sqrt{\alpha(t_1,t_2)}\;dt_1\,dt_2,\quad p,q=1,2,...,N, \tag{19}$$

where α is the determinant of the surface metric tensor. These factors represent the velocity at P_{j}^p induced by a source distribution of density $R_{\mathrm{i}}^p(t_1,t_2)$. Evaluation of Eq. 19 can be achieved by assuming that each induced factor is introduced as:

$$\mathbf{u}_{\mathbf{i}}\left(P_{\mathbf{j}}^p\right)=\mathbf{u}_{\mathbf{i}}^{(nonsing)}\left(P_{\mathbf{j}}^p\right)+\mathbf{u}_{\mathbf{i}}^{(sing)}\left(P_{\mathbf{j}}^p\right) \tag{20}$$

The non-singular integrals are easily calculated by using standard quadrature methods. On the other hand, singular integrals are divided into three cases:

- Far field: Quadrature methods are used as in the non-singular case.
- Near-field: Transformation techniques are used as in Telles (1987) and (1994)
- In-field: Cauchy – Principal Value integrals occur and are evaluated as in Mikhlin (1965).

Integration of the non-singular parts when points P and Q approach the free-surface (z=0) becomes numerically unstable, as observed by Belibassakis et al (2013). As a result, the ship is considered to be furtherly submerged by $dz=\lambda/\alpha$ where λ is the characteristic wave length and α is a number associated with this artificial sinkage. α can be evaluated by numerical experimentation and its value varies for different hull shapes.

The discrete form of BIE (Eq. 15) is

$$\sum_{\mathbf{i}=0}^{\mathbf{n}^p+\mathbf{l}^p}\mu_{\mathbf{i}}^p R^p_{\mathbf{i},\mathbf{l}^p}\left(t^p_{1,j_1},t^p_{2,j_2}\right)-2\Pi(P_{\mathbf{j}}^p)=-2\mathbf{U}\left(P_{\mathbf{j}}^p\right)\cdot\mathbf{n}\left(P_{\mathbf{j}}^p\right),\quad \mathbf{j}=0,....,\mathbf{n}^p+\mathbf{l}^p,\ p=1,...N \tag{21}$$

where

$$\Pi\left(P_{\mathbf{j}}^p\right)=\sum_{q=1}^{N}\sum_{\mathbf{i}=0}^{\mathbf{n}^q+\mathbf{l}^q}\mu_{\mathbf{i}}^q\left[\mathbf{u}_{\mathbf{i}}^q\left(P_{\mathbf{j}}^p\right)\cdot\mathbf{n}\left(P_{\mathbf{j}}^p\right)\right] \tag{22}$$

where $\mathbf{u}_{\mathbf{i}}^q$ are the induced velocity factors and **n** is the unit vector normal to the boundary surface. Convergence usually requires more degrees of freedom than those offered by the representation of the geometric model and thus, the NURBs bases may need refinement. In the context of this

work, knot insertion has been applied (h-refinement) but degree elevation (p-refinement) or both knot insertion and degree elevation (k-refinement) may be utilised.

After the linear system is solved, the velocity of each collocation point can be evaluated by

$$\mathbf{v}\left(P_{\mathbf{j}}^{p}\right)=\mathbf{U}+\mathbf{u}\left(P_{\mathbf{j}}^{p}\right) \tag{23}$$

where $\mathbf{U}$ is the ship's speed and $\mathbf{u}$ is the induced velocity of collocation point $P_{\mathbf{j}}^{p}$ given by

$$\mathbf{u}\left(P_{\mathbf{j}}^{p}\right)=\sum_{q=1}^{N}\sum_{\mathbf{i}=0}^{\mathbf{n}^{q}+\mathbf{l}^{q}}\mu_{\mathbf{i}}^{q}\left(\frac{1}{2}R_{\mathbf{i},\mathbf{l}^{q}}^{q}\left(t_{1,j_1}^{p},t_{2,j_2}^{p}\right)\mathbf{n}\left(P_{\mathbf{j}}^{p}\right)+\mathbf{u}_{\mathbf{i}}^{q}\left(P_{\mathbf{j}}^{p}\right)\right)$$
$$\mathbf{j}=0,....,\mathbf{n}^{p}+\mathbf{l}^{p},\quad p=1,...N \tag{24}$$

And finally the wave resistance can be calculated by

$$C_W=\frac{R_W}{0.5\rho U^2 S_W}=S_W^{-1}\sum_{p=1}^{N}\left(\int_{I_1^p\times I_2^p}C_P n_x\sqrt{a}\;dt_1dt_2\right) \tag{25}$$

where S_W is the wetted surface of the hull, n_x is the x-component of the vector normal to the boundary surface S and C_p is the pressure coefficient given by

$$\mathrm{C_p}=\frac{\mathrm{p}-\mathrm{p}_\infty}{0.5\rho\mathrm{U}^2}=1-\left(|\mathbf{v}|/\mathrm{U}\right)^2-2\mathrm{gz}/\mathrm{U}^2, \tag{26}$$

This method has been implemented for the Wigley and the rebuilt KCS hulls, presented in the previous section. An example of the pressure coefficient distribution on the Wigley hull for F_n=0.316 can be found in the below figure. In this connection it should be stressed that C_p is evaluated directly on the ship hull via the same set of bases functions used for building the CAD model of the hull.

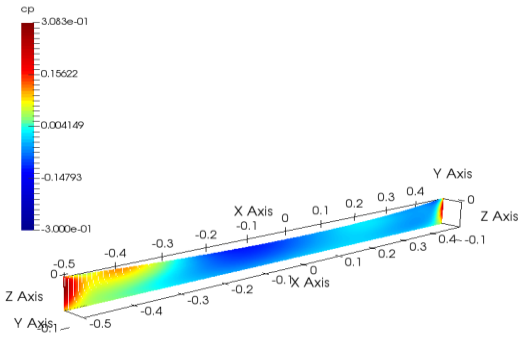

Fig. 12: Pressure coefficient distribution *Cp* over the Wigley hull for F_n=0.316

COMPARISON & CONCLUSIONS

Figures 9 and 10 collect CFD and IGA-BEM estimates of the wave-resistance coefficient for the Wigley hull and the residual-resistance coefficient for the KCS hull. In the latter case, the IGA-BEM estimate for residual resistance is obtained by adding to the wave-resistance coefficient a viscous pressure correction term of the form kC_F, where C_F is the ITTC correlation line (ITTC, 2008a) and k is a form factor that, if not available from experimental data, can be estimated with the support of Prohaska's method and the CFD tool. One can generally assert that the IGA-BEM resistance curves are shape aligned with both the corresponding CFD curves and the experimental data with an average error of 6.4% for the wave resistance estimate over the Froude numbers for which experimental results are available. In this connection, the results of the present preliminary study towards the feasibility of developing a hybrid mid-cost optimisation framework that combines a low-cost IGA-BEM solver with the high-cost CFD one, are not discouraging.

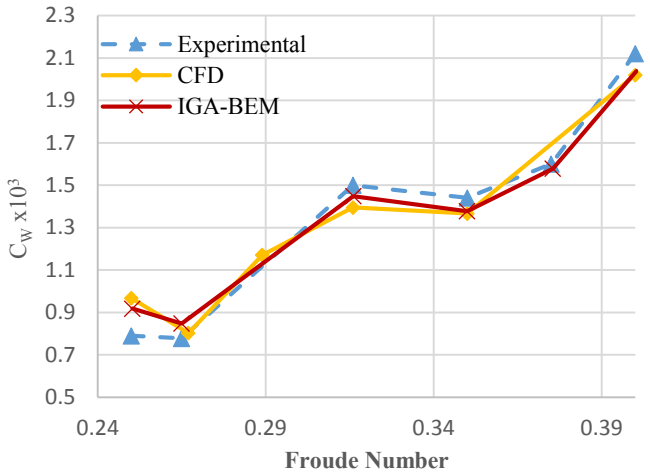

Fig. 13: Simulation & experimental results for the Wigley ship

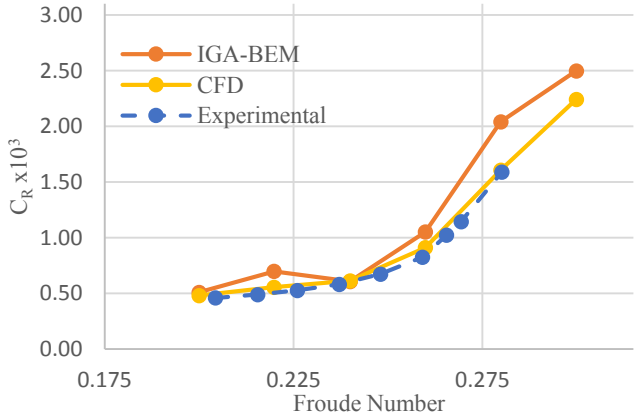

Fig. 14: Simulation and experimental results for the KCS ship

ACKNOWLEDGEMENTS

CFD Results were obtained using the EPSRC funded ARCHIE-WeSt High Performance Computer (www.archie-west.ac.uk). EPSRC grant no. EP/K000586/1. S.P. Chouliaras and P.D. Kaklis received funding from the European Union's Horizon 2020 research and innovation programme under the Marie Skłodowska-Curie grant agreement No 675789

REFERENCES

Baar, JJM, Price, WG (1988). Developments in the Calculation of the Wave-making Resistance of Ships, Proc. *Royal Society of London. Series A*, Mathematical and Physical Sciences 416, No. 1850, 115-147.4195.

Belibassakis, KA, Gerostathis, ThP, Kostas, KV, Politis, CG, Kaklis, PD, Ginnis, AI, Feurer, C (2013). A BEM-isogeometric method for the ship wave-resistance problem. *Ocean Engineering 60*, 53-67.

Brard, R (1972). The representation of a given ship form by singularity distributions when the boundary condition on the free surface is linearized, *J. Ship Res.* 16, 79-82.

Choi, HJ, Chun, HH, Park, IR, Kim, J (2011). "Panel cutting method: new approach to generate panels on a hull in Rankine source potential approximation," International Journal of Naval Architecture and Ocean Engineering, 3(4), 225-232

Farin, GE (1999). Curves and Surfaces for CAGD, A Practical Guide, Fifth Edition, *Morgan Kaufmann Publishers Inc. San Francisco, CA, USA*.

Hughes, TJR, Cottrell, JA, Bazilevs, Y (2005). Isogeometric analysis: CAD, finite elements, NURBS, exact geometry and mesh refinement. *Computer Methods in Applied Mechanics and Engineering* 194, 4135-4195. ITTC (1987). "Report of the Resistance and Flow Committee," In: Proc 18th International Towing Tank Conference, Kobe, Japan, 47-92

ITTC (2008a). "Report of the Resistance Committee," 25th International Towing Tank Conference

ITTC (2008b). "Uncertainty Analysis in CFD Verification and Validation Methodology and Procedures." ITTC – Recommended Procedures and Guidelines, 7.5-03-01-01.

Ju, S (1983). "Study of total and viscous resistance for wigley parabolic ship form. Iowa Institute of Hydraulic Research," Report: IIHR-261

Kim, WJ, Van, DH and Kim, DH (2001). "Measurement of flows around modern commercial ship models", Exp. in Fluids, Vol. 31, pp 567-578

Kostas, KV, Ginnis, AI, Politis, CG and Kaklis, PD, "Ship-Hull Shape Optimization with a Tspline based BEM-Isogeometric Solver", Computer Methods in Applied Mechanics and Engineering, 284, 611-622, (2015).

Launder, BE, Spalding, DB (1974). "The numerical computation of turbulent flows". *Computer Methods in Applied Mechanics and Engineering*. **3** (2): 269–289.

Mikhlin, SG (1965). Multi-Dimensional Singular Integrals and Integral Equations, Pergamon Press. *Engin. Analysis Boundary Elements* 13, 135-141.

Peric, M and Ferziger, JH (2002). "Computational Methods for Fluid Dynamics," Springer, 3rd edition

Prohaska CW (1966). "A simple method for the evaluation of the form factor and the low speed wave resistance," In proceedings of 11th ITTC, International Towing Tank Conference

Telles, JFC (1987). A self-adaptive co-ordinate transformation for efficient numerical evaluation of general boundary element integrals, *Int. Journal Numerical Meth. in Engineering* 24, 959-973.

Telles, JFC, and Oliveira, RF (1994). Third degree polynomial transformation for boundary element integrals: Further improvements, *Engin. Analysis Boundary Elements* 13, 135-141

Wilcox, DC (2008), Formulation of the k–ω Turbulence Model Revisited, **46** (11), AIAA Journal, pp. 2823–2838.